Mini-RPV Lateral Autopilot Design

Itzhack Y. Bar-Itzhack* and Eryk Ferdman†
Technion-Israel Institute of Technology, Haifa, Israel

In this paper the design of a lateral autopilot for a miniature remotely piloted vehicle (RPV) is described. The structure of the autopilot is predetermined, as well as the measured variables. It is shown that, even though aileron alone is used to control the RPV, the system is completely controllable. By use of several indices of performance, the best autopilot gains are determined by minimizing these indices. The minimization is carried out in the complex plane, and comparison is made with state space methods. It is concluded that, when a single error, such as heading error, is considered, the complex plane minimization procedure is superior. It is seen that the RPV poles due to the Dutch-Roll mode stay close to the imaginary axis, although heavy penalty is imposed by the performance index on a persisting error. It is shown that the pole placement is restricted by the fact that the trace of the system matrix is constant. Although no rudder is used, the vehicle executes coordinated turns due to its natural coordination quality. Following the design, an autopilot has been built and tested on a flight table hooked to an analog computer, which simulates the RPV dynamics. The performance of the tested system matched the analog and the digital simulation of the system.

I. Introduction

MINIATURE remotely piloted vehicles have gained considerable interest as battlefield airborne platforms for missions such as surveillance, photoreconnaissance, target acquisition, target location, and jamming of surface to air weapons. In this paper we present the design of an autopilot for such a vehicle which is based on the application of a frequency domain optimization technique.

The trajectory of the vehicle consists of three phases. During the first phase the vehicle is being boosted by a solid propellant motor to an altitude of 6000 ft, where it reaches a velocity of 1.46 Mach. At the beginning of the second phase the motor cuts off. The vehicle continues to gain altitude while losing velocity. At the end of the second phase the vehicle separates from its booster and the elevator jumps to a fixed angle to maintain a constant gliding angle. At the end of this phase the vehicle reaches an altitude of 21,000 ft. and a velocity of 0.45 Mach. During the third phase, the vehicle glides while being guided by a lateral autopilot, whose command inputs are preprogrammed.

II. Autopilot Scheme

Since this is an unmanned vehicle, coordination during turns can be sacrificed for the sake of a simple autopilot. In addition, the Dutch Roll damping is accomplished passively, to a certain extent, by increasing the area of the rudder stabilizer. Consequently, the only active control surfaces are the wing ailerons, which are activated by the autopilot to maintain a desired gliding course. The autopilot scheme, which was chosen for this vehicle (Ref. 1, pp. 157-163), is a rate stabilized lateral autopilot, and shown in Fig. 1. As will be explained in Sec. XII, the choice of a rate stabilized lateral autopilot enables one to use a single rate gyro.

The limiter is needed for preventing the RPV from overturning. Once the configuration of the autopilot has been determined, the remaining problem is a proper selection of gains $K_{\dot\phi}$, $K_{\dot\psi}$, and K_{ψ}. One method for selecting these gains is the root locus (RL) method; however, the application of this method for gain selection involves an enormous amount of trial and error computation, since, while selecting the gains at each loop closure, it is not clear how the selection is going to affect the poles at the end of the process. It is preferable, therefore, to use some optimization technique that assures that the autopilot performs optimally with respect to a selected index of performance. As a by-product of the optimization, the selected gains yield a stable system. To treat the system analytically, one has to formulate the RPV lateral dynamics.

III. Vehicle Lateral Dynamics

The definition of the axes of the vehicle is given in Fig. 2. The authors are interested only in the transfer functions, whose inputs are aileron deflections. The linearized lateral equations of motion of the vehicle about a certain nominal set of axes are derived in Refs. 1 and 2. They are

$$-\frac{b}{2U}C_{y_p}\dot\phi - C_{y_\phi}\phi + \left(\frac{mU}{Sq} - \frac{b}{2U}C_{y_r}\right)\dot\psi - C_{y_\psi}\psi + \frac{mU}{Sq}\dot\beta - C_{y_\beta}\beta = C_{y_a} \tag{1}$$

$$\frac{I_x}{Sqb}\ddot\phi - \frac{b}{2U}C_{\ell_p}\dot\phi - \frac{J_{xz}}{Sqb}\ddot\psi - \frac{b}{2U}C_{\ell_r}\dot\psi - C_{\ell_\beta}\beta = C_{\ell_a} \tag{2}$$

$$-\frac{J_{xz}}{Sqb}\ddot\phi - \frac{b}{2U}C_{n_p}\dot\phi + \frac{I_z}{Sqb}\ddot\psi - \frac{b}{2U}C_{n_r}\dot\psi - C_{n_\beta}\beta = C_{n_a} \tag{3}$$

The C coefficients are the nondimensional lateral stability derivatives.

In the present case, as in many others, the stability derivatives C_{y_p} and C_{y_r} are negligible. In addition, in this case J_{xz}, C_{y_ψ}, $C_{y_{\delta_a}}$ and $C_{n_{\delta_a}}$ are negligible too. Also note that, since there is no rudder control $\delta_r = 0$. Denote

$$a_1 = -C_{y_\phi} \quad a_2 = mU/Sq \quad a_3 = -C_{y_\beta}$$

$$b_1 = -(b/2U)C_{n_p} \quad b_2 = I_z/Sqb \quad b_3 = -(b/2U)C_{n_r}$$

$$b_4 = -C_{n_\beta} \quad c_1 = I_x/Sqb \quad c_2 = -(b/2U)C_{\ell_p}$$

$$c_3 = -(b/2U)c_{\ell_r} \quad c_4 = -c_{\ell_\beta} \quad f = C_{\ell_{\delta_a}} \tag{4}$$

Presented as Paper 75-1121 at the AIAA Guidance and Control Conference, Boston, Mass., Aug. 20-22, 1975; submitted Sept. 10, 1975; revision received March 15, 1976. The authors wish to thank S. J. Merhav for providing most of the equipment needed for performing the experimental part of this work and for his encouragement. They also wish to thank R. Sivan for his helpful comments and advice.

Index categories: Aircraft Handling, Stability, and Control; Navigation, Control, and Guidance Theory.

*Senior Lecturer, Dept. of Electrical Engineering. Member AIAA.
†Graduate Student, Dept. of Electrical Engineering.

Then Eqs. (1-3) can be written as

$$a_1\phi+a_2\dot{\psi}+a_2\dot{\beta}+a_3\beta=0 \tag{5}$$

$$b_1\dot{\phi}+b_2\ddot{\psi}+b_3\dot{\psi}+b_4\beta=0 \tag{6}$$

$$c_1\ddot{\phi}+c_2\dot{\phi}+c_3\dot{\psi}+c_4\beta=f\delta_a \tag{7}$$

Rearranging the last three equations, one obtains

$$\dot{\beta}=-\frac{a_3}{a_2}\beta-\dot{\psi}-\frac{a_1}{a_2}\phi \tag{8}$$

$$\ddot{\psi}=-\frac{b_4}{b_2}\beta-\frac{b_3}{b_2}\dot{\psi}-\frac{b_1}{b_2}\dot{\phi} \tag{9}$$

$$\ddot{\phi}=-\frac{c_4}{c_1}\beta-\frac{c_3}{c_1}\dot{\psi}-\frac{c_2}{c_1}\dot{\phi}+\frac{f}{c_1}\delta_a \tag{10}$$

The equation of the aileron servo is

$$\dot{\delta}_a=-\Omega\delta_a+\alpha e_a \tag{11}$$

As shown in Fig. 1, the following control law has been chosen:

$$e_a=K_\psi(\psi_{\text{ref}}-\psi)-K_{\dot{\psi}}\dot{\psi}-K_{\dot{\phi}}\dot{\phi} \tag{12}$$

The authors consider the autopilot as a regulating system, with ψ_{ref} being the constant set point. In the optimization process, the same gains will be obtained if a nonzero initial condition of ψ and a zero ψ_{ref} is chosen;[3] thus Eq. (12) becomes

$$e_a=-K_\psi\psi-K_{\dot{\psi}}\dot{\psi}-K_{\dot{\phi}}\dot{\phi} \tag{13}$$

The following state variables are defined:

$$x_1=\beta \qquad x_2=\psi \qquad x_3=\dot{\psi}=\dot{x}_2$$

$$x_4=\phi \qquad x_5=\dot{\phi}=\dot{x}_4 \qquad x_6=\delta_a \tag{14}$$

Augmenting Eqs. (8-11 and 14), one obtains the following state space representation of the aileron controlled RPV:

$$\dot{x}=\tilde{A}x+Bu \tag{15}$$

where

$$\tilde{A}=\begin{bmatrix} -a_3/a_2 & 0 & -1 & -a_1/a_2 & 0 & 0 \\ 0 & 0 & 1 & 0 & 0 & 0 \\ -b_4/b_2 & 0 & -b_3/b_2 & 0 & -b_1/b_2 & 0 \\ 0 & 0 & 0 & 0 & 1 & 0 \\ -c_4/c_1 & 0 & -c_3/c_1 & 0 & -c_2/c_1 & f/c_1 \\ 0 & 0 & 0 & 0 & 0 & -\Omega \end{bmatrix} \tag{16a}$$

$$B=\begin{bmatrix} 0 \\ 0 \\ 0 \\ 0 \\ 0 \\ 1 \end{bmatrix} \qquad u=\alpha e_a \tag{16b}$$

The output of interest is merely ψ; hence, define an output matrix H as follows:

$$H=[0\ 1\ 0\ 0\ 0\ ] \tag{17}$$

Thus, the output equation is

$$x_2=Hx \tag{18}$$

In addition, define a vector z of the measured variables and a measurement matrix C as follows:

$$z=\begin{bmatrix} x_2 \\ x_3 \\ x_5 \end{bmatrix} \qquad C=\begin{bmatrix} 0 & 1 & 0 & 0 & 0 & 0 \\ 0 & 0 & 1 & 0 & 0 & 0 \\ 0 & 0 & 0 & 0 & 1 & 0 \end{bmatrix} \tag{19}$$

Hence, the measurement equation is

$$z=Cx \tag{20}$$

Finally, define the row matrix K as follows

$$K=[K_\psi \quad K_{\dot{\psi}} \quad K_{\dot{\phi}}] \tag{21}$$

Then, from Eqs. (13, 16, 19, and 21), one obtains the feedback equation

$$u=-\alpha\ Kz \tag{22}$$

IV. Controllability

Before proceeding with optimization, we wish to examine the controllability of the system. There are two reasons for this; first, to discover whether an aileron-controlled vehicle can reach any desired ψ in a finite time interval, and second, a solution to an optimal control problem may not exist if the system considered is not controllable (Ref. 4, p. 755). The authors are interested in the question of whether the system is completely output controllable. The answer to this question is positive if, and only if, the matrix

$$[H\,|H\tilde{A}B|H\tilde{A}^2B|\cdots|H\tilde{A}^5B|O]$$

is of rank one, that is, if there is at least one nonzero element in the last row matrix. It can be seen that this condition is met if, for example, $C_{l_{\delta_a}}\neq 0$ and $C_{n_p}\neq 0$. In fact, it also can be shown that in this case the rank of the matrix

$$[B\,|\tilde{A}B|\cdots|\tilde{A}^5B]$$

is 6; thus, the present system also is completely state-controllable.

V. Indices of Performance

As was mentioned earlier, a nonzero initial condition was chosen for ψ and a zero ψ_{ref}, thus, $\psi(t)$ also is the error $\psi(t)$. A logical index of performance is

$$I_0=\int_0^\infty \psi^2(t)\ \mathrm{d}t \tag{23}$$

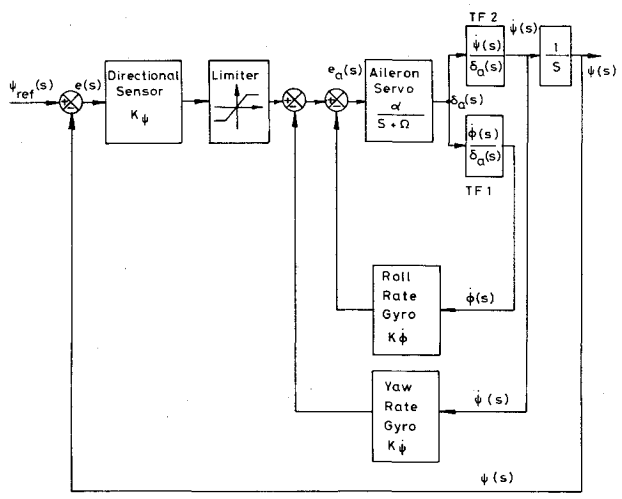

Fig. 1 Block diagram of the rate stabilized lateral autopilot.

If one wants to impose a penalty on a sustained error, he can choose

$$I_1=\int_0^\infty t\ \psi^2(t)\ \mathrm{d}t$$

The latter index is analytically hard to handle; thus, the authors prefer to use

$$I_2=\int_0^\infty t^2\ \psi^2(t)\ \mathrm{d}t \tag{24}$$

or any other index with an even power of t; namely,

$$I_n=\int_0^\infty t^n\ \psi^2(t)\ \mathrm{d}t \tag{25}$$

where n is even.

VI. Minimization Procedure

In all of the minimization methods, which we will describe later, the following search method will be used. We have chosen randomly a set of gains K_ψ, $K_{\dot\psi}$, and $K_{\dot\phi}$. We fixed $K_{\dot\psi}$ and $K_{\dot\phi}$ and changed K_ψ in steps. For every step, we found the poles of the closed-loop system. In case any of the poles was on the $j\omega$ axis or at the right-hand side of the complex plane, we set the value of the corresponding performance index to -1 and went on to the next step. If all of the poles were stable, we computed the index of performance for that step and went on to the next step. when a nonnegative minimum of the index of performance for changes in K_ψ was attained, we fixed K_ψ at that value and then moved on to minimize over $K_{\dot\psi}$. When a minimum over $K_{\dot\psi}$ was attained, we went back to minimize over K_ψ until the process converged to a point in the $K_\psi K_{\dot\psi}$ plane. Only then, and for this point, we minimized over $K_{\dot\phi}$ and, as minimum was reached, we fixed $K_{\dot\phi}$ and repeated the process. Eventually the process converged to a point in the K_ψ, $K_{\dot\psi}$, $K_{\dot\phi}$ space for which a local minimum of the index of performance was found. The final search cycle generated graphs of the index of performance I_n vs the gains. The most sophisticated, as well as time-consuming, part of the minimization process was the evaluation of I_n at each step.

VII. State Space Computation of I_n

The state space computation of I_n is based on the fact[5] that, for the stable system,

$$\dot x=Ax \tag{26}$$

and for a positive definite matrix Q, the following relationship holds:

$$\int_0^{t_f} x^t(t)Q(t)x(t)\,\mathrm{d}t=x^t(0)P(0)x(0) \tag{27}$$

where $P(0)$ is the initial value of the maxtix $P(t)$, which is the solution of the matrix differential equation

$$\dot P(t)=-A^tP(t)-P(t)A-Q(t)\qquad P(t_f)=\theta \tag{28}$$

To use Eq. (27) and (28), the system must be expressed in the form of Eq. (26). We observe that Eqs. (15, 20, and 22) can be augmented to the following closed-loop system state space representation:

$$\frac{d}{dt}\begin{bmatrix}x_1\\x_2\\x_3\\x_4\\x_5\\x_6\end{bmatrix}=\begin{bmatrix}-a_3/a_2 & 0 & -1 & -a_1/a_2 & 0 & 0\\ 0 & 0 & 1 & 0 & 0 & 0\\ -b_4/b_2 & 0 & -b_3/b_2 & 0 & -b_1/b_2 & 0\\ 0 & 0 & 0 & 0 & 1 & 0\\ -c_4/c_1 & 0 & -c_3/c_1 & 0 & -c_2/c_1 & f/c_1\\ 0 & -K_\psi\alpha & -K_{\dot\psi}\alpha & 0 & -K_{\dot\phi}\alpha & -\Omega\end{bmatrix}\begin{bmatrix}x_1\\x_2\\x_3\\x_4\\x_5\\x_6\end{bmatrix} \tag{29}$$

The matrix A is, of course, a function of K_ψ, $K_{\dot\psi}$, and $K_{\dot\phi}$. We note that, if Q is chosen as

$$Q=\begin{bmatrix}0 & & & & & \\ & 1 & & & & \\ & & 0 & & & \\ & & & 0 & & \\ & & & & 0 & \\ & & & & & 0\end{bmatrix}$$

and if, in addition, $t_f\to\infty$, then the left-hand side of Eq. (27) is identical to I_0 defined by Eq. (23). Therefore,

$$I_0=x^t(0)P(0)x(0) \tag{30}$$

As mentioned eariler, of all of the elements of $x(0)$, only $\psi(0)$ is nonzero; hence, with no loss of generality, we may choose $\psi(0)=1$, and write

$$x^t(0)=[0\ 1\ 0\ 0\ 0\ 0\ ] \tag{31}$$

Thus Eq. (30) becomes

$$I_0=p_{22}(0)$$

where $p_{22}(0)$ is the 2, 2 element of $P(0)$. It can be shown [Ref. 3, p. 111] that, for the case in which A and Q are constant matrices, P also is a constant matrix, which solves Liapunov's algebraic equation

$$A'P+PA+Q=\theta$$

If one sets

$$Q=\begin{bmatrix} 0 & & & & & \\ & t^n & & & & \\ & & 0 & & & \\ & & & 0 & & \\ & & & & 0 & \\ & & & & & 0 \end{bmatrix}$$

then the left-hand side of Eq. (27) is identical to I_n defined by Eq. (25); hence,

$$I_n=x'(0)P(0)x(0) \tag{32}$$

and $P(0)$ is computed using Eq. (28) as follows.

The final time is chosen such that it is large enough to let all of the transients die out; thus,

$$\int_{t_f}^{\infty} t^2\psi^2(t)\,dt=\int_{t_f}^{\infty} x'(t)Q(t)x(t)\,dt\to 0$$

Set

$$P(t_f)=\theta$$

and, using Eq. (28), we integrate $P(t)$ backwards until $t=0$. We use Euler's method for integration, since it is the simplest method, to improve the accuracy of the computation, we make use of the fact that $P(t)$ is symmetric, and symmetrize the resultant matrix after each integration step.[6] Thus, the computation cycle is

$$\tilde{P}_{n+1}=P_n+(A'P_n+P_nA+Q_m)\Delta t$$

$$P_{n+1}=\tfrac{1}{2}(\tilde{P}_{n+1}+\tilde{P}'_{n+1})$$

starting at $P_0=\theta$ and terminating at $N=t_f/\Delta t$. From Eqs. (31) and (32), we conclude that the 2,2 term of P_n is I_n, as defined by Eq. (25).

VIII. Frequency Domain Computation of I_n

The computation of I_n in the state space is rather time-consuming. In the present work we preferred to use the frequency domain computation method, which is based on Parseval's theorem. First, we need to find the Fourier transform of $\psi(t)$. Thus we transform Eqs. (1-3) and solve the transformed equations to get

$$\frac{\dot{\phi}(s)}{\delta_a(s)}=\frac{A_ps^3+B_ps^2+C_ps}{\Delta(s)} \tag{33}$$

$$\frac{\dot{\psi}(s)}{\delta_a(s)}=\frac{A_rs^3+B_rs^2+C_rs+D_r}{\Delta(s)} \tag{34}$$

where

$$\Delta(s)=\bar{A}s^4+\bar{B}s^3+\bar{C}s^2+\bar{D}s+\bar{E} \tag{35}$$

The expressions for the coefficients

$$\bar{A},\ A_p,\ A_r,\bar{B},\ B_p,B_r,\ \bar{C},C_p,C_r,\bar{D},D_r$$

and $\bar{E}$ are given in Ref. 2. To these equations, add the aileron-servo equation

$$\delta_a(s)/e_a(s)=\alpha/(s+\Omega) \tag{36}$$

and the following transformed feedback equation (see Fig. 1):

$$e_a(s)=K_\psi e(s)-K_{\dot{\psi}}s\psi(s)-K_{\dot{\phi}}s\phi(s) \tag{37}$$

As stated earlier,[3] the system error will be exactly the same in absolute value, whether $\psi_{\text{ref}}=0$ and $\psi(0)=1$ or $\psi_{\text{ref}}=1$ and $\psi(0)$. We choose the latter alternative and write

$$e(s)=(1/s)-\psi(s) \tag{38}$$

Augmentation of Eqs. (33-38) yields the Fourier transform of $e(s)$. We realize that, in view of the two equivalent alternatives,

$$I_n=\int_0^{\infty} t^ne^2(t)\ dt \tag{39}$$

In particular,

$$I_0=\int_0^{\infty} e^2(t)\ dt \tag{40}$$

To evaluate Eq. (40) we use Parseval's theorem,[7] according to which

$$\int_{t=-\infty}^{t=\infty} y^2(t)\,dt=\frac{1}{2\pi j}\int_{s=-j\infty}^{s=j\infty} Y(s)\,Y(-s)\,ds \tag{41}$$

where $Y(s)$ is the Fourier transform of $y(t)$; hence, from Eqs. (40) and (41),

$$I_0=\frac{1}{2\pi j}\int_{-j\infty}^{j\infty} e(s)e(-s)\,ds \tag{42}$$

In this case, $e(s)$ is a rational function, whose denominator polynomial is of the order of 6; hence, we use a formula given in Appendix E of Ref. 7 to evaluate Eq. (42). To calculate I_2 we make use of the well-known theorem of the Fourier transform which states that

$$\mathfrak{F}\{te(t)\}=-(\mathrm{d}/\mathrm{d}s)e(s)$$

Then in view of Eq. (41),

$$\int_{t=-\infty}^{t=\infty}[te(t)]^2\,dt=\frac{1}{2\pi j}\int_{s=-j\infty}^{s=j\infty}\left[\frac{\mathrm{d}}{\mathrm{d}s}e(s)\right]\left[\frac{\mathrm{d}}{\mathrm{d}s}e(-s)\right]ds$$

Hence,

$$I_2=\frac{1}{2\pi j}\int_{-j\infty}^{j\infty}\left[\frac{\mathrm{d}}{\mathrm{d}s}e(s)\right]\left[\frac{\mathrm{d}}{\mathrm{d}s}e(-s)\right]ds \tag{43}$$

The denominator polynomial of $\mathrm{d}/\mathrm{d}s[e(s)]$ is of the order of 12, and unfortunately there are no ready formulas to evaluate Eq. (43); hence, we had to solve a set of linear algebraic equations[7,8] to calculate I_2. At any rate, this was done much faster than the solution of Eq. (28), which was described in Sec. VII. It should be noted that the frequency domain computation of I_n also can be accomplished by use of the complex convolution theorem of the Laplace transform, rather than the complex differentiation theorem used here.[9]

IX. Results

The minimization process was carried out on an IBM 370/168 digital computer. The method that has been used was

Table 1 Optimal gains

Performance index used in the optimization	Designation of the corresponding local minimum	K_ψ	$K_{\dot\psi}$	$K_{\dot\phi}$
I_0	L_1	404	210	3.6
	L_2	156000	10000	215
I_2	L_1	250	177	3.24
	L_2	21360	10350	213
	L_3	286	242	8.5
H	L_3	300	250	9

Table 2 Optimal indices of performance

		Obtained by		
		Complex plane optimization	State space optimization	CSMP simulation and actual integration
I_0	L_1	0.52914	0.52472	0.52635
	L_2	0.20625	0.20630	0.20995
I_2	L_1	0.12777	0.12227	0.12233
	L_2	0.02526	0.05636	0.05593
	L_3	0.35035	0.31946	0.32655

the frequency domain method of computation of I_n, defined in Eq. (42) for I_0 and in Eq. (43) for I_2. The results of the search yielded a set of gains and the corresponding value of the index of performance. The correspondence between the gains and the index of performance was checked by use of the state space technique [Eq. (30) and (32)]. The results also have been verified through simulation (using IBM's CSMP digital simulation program) and integration of $\psi^2(t)$, which yielded the correct index of performance.

A final verification of the design was carried out on the autopilot hardware. The autopilot cluster of sensors was mounted on a flight table, and the RPV transfer functions were simulated on an EAI 580 analog computer. The aileron angle was measured on the actuator axis and fed into the computer setup. The resulting attitude angles were fed back from the computer into the flight table, which turned the sensor cluster to the right attitude. The aileron and attitude angles were recorded and compared with the corresponding angles, which were recorded when the whole system, including the autopilot, was simulated on the analog computer. These aileron and attitude angles also were compared with the corresponding angles, which were the outcome of a completely digital simulation, using CSMP simulation language. The gains of six cases that we have considered are tabulated in Table 1. I_0 indicates that the index of performance was

$$\int_0^\infty t\ \psi^2(t)\,dt$$

I_2 indicates that the index of performance was

$$\int_0^\infty t^2\psi^2(t)\,dt$$

H indicates the case I_2L_3 after adjustment to the actual hardware. For each index of performance, more than one local minimum were found. L_1, L_2, and L_3 denote the local minima that have been found. The corresponding indices of performance, as verified by three different methods, are shown in Table 2.

We first obtained the case I_0L_1, whose performance is demonstrated in Fig. 3, where the response of the system to a step change of ψ_{ref} has been recorded. A smaller index of performance was obtained at I_0L_2; however, the aileron motion

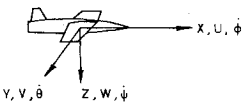

axis	direction	linear velocity	angular velocity	small angular velocity	angular displacement
OX	forward	U	P	$\dot\phi$	ϕ
OY	right wing	V	Q	$\dot\theta$	θ
OZ	downward	W	R	$\dot\psi$	ψ

axis	moment of inertia	product of inertia	force	moment
OX	I_x	$J_{xy}=0$	F_x	L_x
OY	I_y	$J_{yz}=0$	F_y	M_y
OZ	I_z	$J_{zx}=0$	F_z	N_z

Fig. 2 Definition of axes and variables.

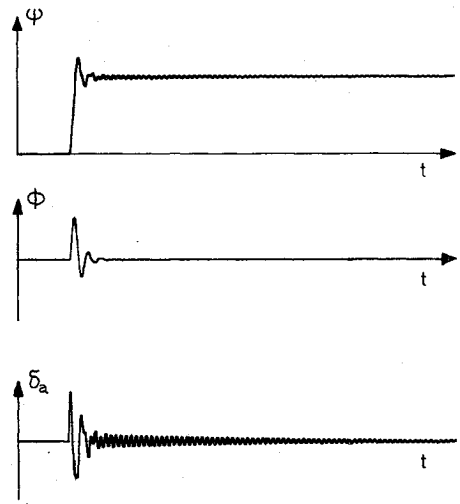

Fig. 3 System response to a step of ψ_{ref}, case I_0L_1.

was too oscillatory during the transient period. This local minimum is achieved when very high gains are used. The value of the functional I_n is then the smallest, and the dominant poles are far from the origin, but close to the imaginary axis; hence, their damping is small. In order to reduce the settling time of the system at the expense of the error, at the beginning of the transient period, we introduced I_2, the ITSES performance index. Minimization of I_2 rather than of I_0 did indeed decrease the settling time, as can be seen in Fig. 4, in which the system response for case I_2L_1 has been recorded. However, we see that, in spite of the heavy penalty imposed on prolonged transients, the response exhibits a lightly damped mode, which is still evident, even when we minimize

$$I_4=\int_0^\infty t^4\psi^2(t)\,dt$$

As with I_0L_2, we found the local minimum I_2L_2 for which I_2, the index of performance, was smaller than that of I_2L_1, but here too the behavior of the aileron was too oscillatory. Still a third local minimum was found for which I_2 was larger than that of the other local minima; however, the hardware response for gains that were found in this case (which we denoted by I_2L_3) was the best. Figure 5 shows the response of the autopilot hardware hooked to the analog computer, where the gains correspond to case H, and Fig. 6 shows the response of the system to a 30 deg offset in ψ_{ref}. Here the limiter goes into action, and the system is highly nonlinear.

A sensitivity analysis was carried out on case I_2L_3. It was found that even a one at a time change of $\pm 20\%$ in the aerodynamic coefficients of the RPV did not drive the autopiloted vehicle unstable. The autopiloted RPV performance also was checked at sea level conditions with the op-

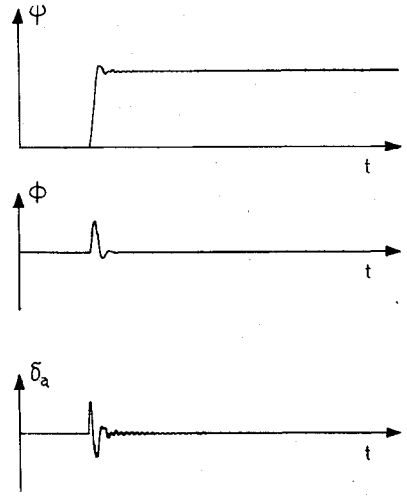

Fig. 4 System response to a step of ψ_{ref}, case I_2L_1.

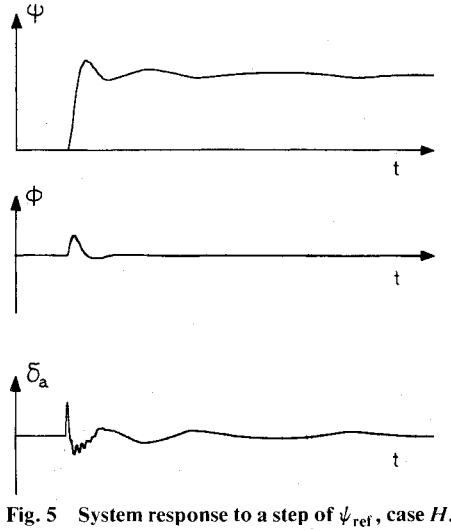

Fig. 5 System response to a step of ψ_{ref}, case H.

timal gains of case I_2L_3 and it was found to be even better than at 20,000 ft.

X. Pole Location

Figure 7 shows the locus of the poles of the local minimum L_1 as they move with the power of t in the index of performance. Note that the poles due to the Dutch-Roll mode hardly move, although a high penalty is imposed by I_4 on sustained oscillations. Moreover, observe that when the two upper branches of the pole locus in Fig. 7 move to the left, as expected, the lower branch moves to the right. To explain this phenomenon, we turn to Eq. (26), the closed-loop state equation of the linear system $\dot{x}=Ax$. The poles of the system are the eigenvalues of A. Denote these eigenvalues by λ_i, $i=1,2,\ldots,6$ and recall the well-known relation

$$\sum_{i=1}^{6} \lambda_i = \text{trace } \{A\}$$

Calculating the trace of $\{A\}$ from Eq. (29), the last equation becomes

$$\sum_{i=1}^{6} \lambda_i = -\left[\frac{a_3}{a_2}+\frac{b_3}{b_2}+\frac{c_2}{c_1}+\Omega\right] = \text{const} \qquad (44)$$

It is seen that the sum of the poles (eigenvalues) must stay constant; thus, if for a certain set of optimal gains two poles move to the left, one pole has to move to the right to satisfy

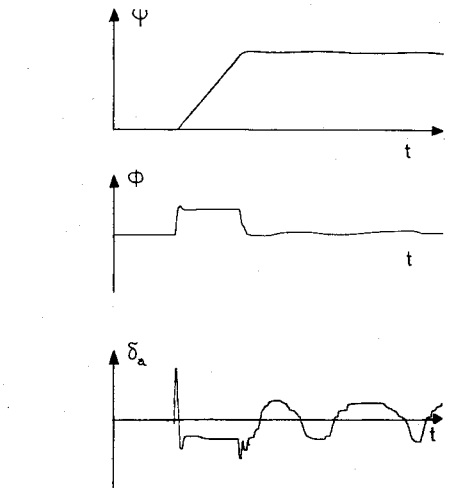

Fig. 6 Nonlinear system response to a large step of ψ_{ref} (hardware response).

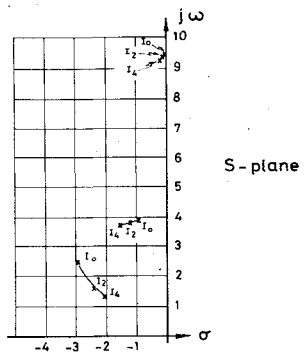

Fig. 7 Pole movement associated with the L_1 local minimum as a function of the order of the performance index (only upper half is shown).

Eq. (44). Although we are restricted in the pole placement of the system, we are quite satisfied with the performance achieved with the poles where they are. If it is desired to change the constant of Eq. (44), one may try to increase Ω. This would mean decreasing the aileron servo time constant, a goal that may be hard to achieve. An increase in Ω means an increase of the agility of the aileron servo and an increase in the damping of the system.

XI. Natural Coordination

In some cases, when certain relationships between the coefficients of the vehicle hold, its yaw rate response to aileron deflections is proportional to the bank angle response. In this case, the vehicle exhibits natural coordination. The general conditions for the existence of this quality now will be examined. From Eqs. (3) and (34), we may write

$$\frac{\dot{\psi}(s)}{\phi(s)} = \frac{\dot{\psi}(s)}{\delta_a(s)} \Big/ \frac{\phi(s)}{\delta_a(s)} = \frac{A_r s^3 + B_r s^2 + C_r s + D_r}{A_p s^2 + B_p s + C_p} \qquad (45)$$

For Eq. (45) to be approximately a constant, two basic conditions must exist, namely: A_r must vanish, and the zeros of the remaining second-order polynomial must be close to those of the denominator polynomial. It can be shown that the condition for which A_r vanishes is

$$C_{n\delta_a} = 0$$

In the present case, this coefficient indeed is zero. A check of the numerical values of the remaining numerator polynomial roots reveals that they are very close to the denominator roots; moreover, it can be shown that in this case $D_r/C_p \simeq g/U'$ which is indeed the ratio between $\dot{\psi}$ and ϕ when a coordinated turn is executed.

XII. Rate Gyro Arrangement

It has been suggested[10] that a single rate gyro be used to measure $\dot{\psi}$ and $\dot{\phi}$. This can be done by installing a rate gyro whose sensitive axis is tripped away from the yaw axis by an angle Γ toward the roll axis. In this way the gyro measurement g is given by

$$g=\dot{\psi}\ \cos\Gamma+\dot{\phi}\ \sin\Gamma \tag{46}$$

Denote the output of the limiter of Fig. 1 by L; then, obviously,

$$e_a=L-(\dot{\psi}K_{\dot{\psi}}+\dot{\phi}K_{\dot{\phi}}) \tag{47}$$

If, instead of feeding back the output of the two rate gyros of Fig. 1, we feed back the output of the tipped away single gyro through a gain K, we obtain, using Eq. (46)

$$e_a=L-K(\dot{\psi}\ \cos\Gamma+\dot{\phi}\sin\Gamma) \tag{48}$$

Comparison of Eqs. (47) and (48) reveals that the single rate gyro arrangement is equivalent to the two rate gyro arrangement of Fig. 1, provided that

$$K\ \cos\Gamma=K_{\dot{\psi}} \tag{49a}$$

$$K\ \cos\Gamma=K_{\dot{\phi}} \tag{49b}$$

Dividing Eq. (49b) by Eq. (49a) yields $\tan\Gamma=K_{\dot{\phi}}/K_{\dot{\psi}}$. Hence, the necessary tipping angle is given by

$$\Gamma=\tan^{-1}K_{\dot{\phi}}/K_{\dot{\psi}} \tag{50}$$

Squaring Eqs. (49a) and (49b), and then adding the two resultant equations, yields the necessary gain

$$K=(K_{\dot{\psi}}{}^2+K_{\dot{\phi}}{}^2)^{1/2} \tag{51}$$

By use of the hardware adjusted values obtained for $K_{\dot{\psi}}$ and $K_{\dot{\phi}}$ we obtain from Eqs. (50) and (51), $\Gamma=2.05$ deg. and $K=250.07$.

It should be noted that, in the present case, where the RPV possesses the natural coordination quality, an alternative method exists for eliminating one rate gyro. This is done by measuring $\dot{\phi}$ only and then deriving $\dot{\psi}$ by passing the measured value of $\dot{\phi}$ through a low pass filter whose time constant is large.

XIII. Conclusions

It has been shown that, because the aileron-controlled Mini-RPV constitutes a controllable system, a simple autopilot, which is based on a single control through the ailerons and the measurement of a single rate-gyro, performs satisfactorily. An optimal design of the autopilot gains, which is based on the minimization of the ITSES performance index, yields a stable system with good performance, although the poles due to the Dutch-Roll mode are close to the imaginary axis and cannot be placed arbitrarily in the complex plane. It was found that an increase in the agility of the aileron servo increases the system damping.

Optimization using the ITSES criterion is performed much faster in the complex plane than it is in the state space, as long as a single error is considered. The incorporation of additional errors in the performance index is straightforward. A more detailed description of the work reported on in this paper can be found in Ref. 11.

References

[1] Blakelock, H. J., *Automatic Control of Aircraft and Missiles*, Wiley, New York, 1965.

[2] McRuer, D., Ashkenas, I., and Graham, D., *Aircraft Dynamics and Automatic Control*, Princeton University Press, Princeton, N.J., 1973.

[3] Kwakernaak, H. and Sivan, R., *Linear Optimal Control Systems*, Wiley-Interscience, New York, 1972.

[4] Ogata, K., *Modern Control Engineering*, Printice-Hall, Englewood Cliffs, N.J., 1970.

[5] Jameson, A., "Optimization of Linear Systems of Constrained Configuration," *International Journal of Control*, Vol. 11, 1970, pp. 409-421.

[6] Bucy, R. S. and Joseph, P. D., *Filtering for Stochastic Processes with Application to Guidance*, Wiley-Interscience, New York, 1968.

[7] Newton, Jr., G. C., Gould, L. A., and Kaiser, J. F., *Analytic Design of Linear Feedback Controls*, Wiley, New York, 1957.

[8] Booton, R. C., Jr., Mathews, M. V., and Seifert, W. W., "Nonlinear Servomechanisms with Random Inputs," Rept. 70, MIT Dynamic Analysis and Control Laboratory, Aug. 20, 1953.

[9] Westcott, J. H., "The Minimum Moment of Error-Squared Criterion: New Performance Criterion for Servos," *Proceedings of the IEEE*, Vol. 101, Pt. II, 1954, pp. 471-480.

[10] Colby, S. J., Franklin, C. E., and Prins, D. W. S., "Command and Control Challenge for RPVs," *Astronautics & Aeronautics*, Vol. 12, Sept. 1974, pp. 64-70.

[11] Ferdman, E., "Design Simulation and Testing of an Optimal Lateral Autopilot," M.Sc. project thesis, Technion-Israel Institute of Technology, April 1975.